Materials and Structures/Matériaux et Constructions, Vol. **35**, June 2002, pp 262-278

RILEM TECHNICAL COMMITTEES

RILEM TC 162-TDF: TEST AND DESIGN METHODS FOR STEEL FIBRE REINFORCED CONCRETE

Design of steel fibre reinforced concrete using the σ-w method: principles and applications

The text presented hereafter is a draft for general consideration. Comments should be sent to the TC Chairlady: Prof. dr. ir. Lucie Vandewalle, K.U. Leuven, Department Burgerlijke Bouwkunde, Kasteelpark Arenberg 40, 3001 Heverlee, Belgium. Fax: +32 16 321976; e-mail: lucie.vandewalle@bwk.kuleuven.ac.be, by 31 October 2002.

TABLE OF CONTENTS

1. SCOPE

The design principles described in the following are based on the fracture mechanical approach known as the fictitious crack model, which relies on the so-called stress-crack opening relationship $\sigma_w(w)$ as the basic material input.

The design method is applicable for Steel Fibre Reinforced Concretes (SFRC) that exhibit *tension softening behaviour*. The method can also be used for other Fibre Reinforced Cementitious Composites (FRCC) that exhibit tension softening behaviour as well as plain concrete (which is assumed always to exhibit tension softening behaviour).

The following cases are covered in this document:

- Cross section subject to combination of axial force, bending moment and shear force. Reinforcement can be a combination of conventional re-bars and fibres.
- Slab on grade subjected to shrinkage.

2. BACKGROUND

2.1 Mechanics of crack formation and propagation

When unreinforced concrete fails in uniaxial tension the failure is governed by the formation of a single crack.

When a crack is formed in fibre reinforced concrete, the fibres will typically stay unbroken. The fibres crossing a crack will resist further crack opening and impose what is called crack closing or crack bridging effect on the crack surfaces. Different failure modes can result, depending on the effectiveness of the fibres in providing crack bridging, see Fig. 1. If the fibres break or are pulled out during crack initiation, or if the fibres cannot carry more load after the formation of the first through crack, then the first cracking strength is the ultimate strength and further deformation is governed by the opening of a single crack and fibres pulling out and/or breaking along the edges of the crack, see Fig. 1(a). This behaviour is also know as tension softening behaviour. If – on the other hand – the fibres are able to sustain more load after the formation of the first crack, more cracks will be formed and what is known as multiple cracking, see Fig. 1(b). This behaviour is also known as strain (or pseudo-strain) hardening behaviour. In the present text only materials exhibiting the first type of behaviour will be dealt with.

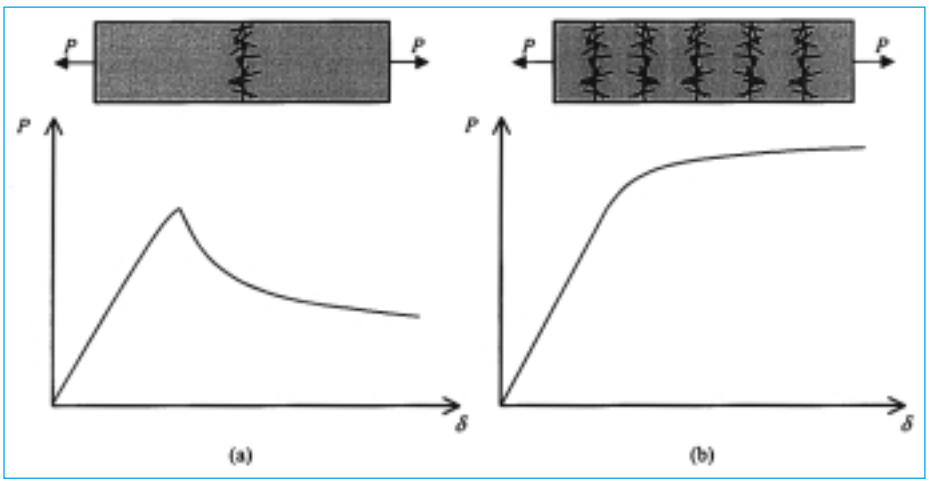

Fig. 1 - The principle of single and multiple cracking. The specimens are loaded in uniaxial tension and the schematic load versus deformation, $P(\delta)$, relationship is shown together with the cracking pattern. The left hand side (a) shows single cracking (or tension softening) while the right hand side shows multiple cracking (or strain hardening).

2.2 Fracture mechanics for concrete

Fracture mechanics deals with the mechanics of crack formation and propagation in materials. When structures are made from softening materials, crack formation often governs the structural behaviour.

Fracture mechanics of concrete is a relatively young scientific and engineering field compared *e.g.* to fracture mechanics of metals. The first significant attempts to develop a non-linear fracture mechanics framework for concrete were taken in the nineteen sixties after it had been realized that linear fracture mechanics could not be applied. Excellent text books are now available on the subject [13, 31, 8].

Conceptually, a crack propagating in concrete is modelled by a zone of diffuse microcracking - the process zone, and a localized crack. The localized crack can be divided into a part where aggregate interlock is present, and a "true" traction free crack. A remarkably simple description of crack formation in plain concrete was suggested by [12]. Hillerborg suggested the so-called Fictitious Crack Model (FCM) which originally was intended for use in combination with FEM. However, as it will be shown here the approach can easily be adopted in other numerical and analytical models.

The fictitious crack model relies on a number of simple assumptions:

1. Only bridging traction normal to the fracture plane is considered.

2. Process zone[1], localized crack with aggregate interlock and localized stress free crack can be modelled by a single crack plane.

3. The process zone, together with the part of the localized crack where aggregate interlock is present is referred to as the fictitious crack. The mechanical behaviour of the fictitious crack is characterized by the stress-crack opening relationship, $\sigma_w(w)$, where σ_w is the traction applied to the crack surface as a function of crack opening w.

4. Stress-singularities[2] can be disregarded. As soon as the largest principal stress reaches the tensile strength a fictitious crack is formed.

5. The length of the fictitious crack cannot be assumed to be small compared with a typical structural dimension.

In Fig. 2, a real crack in plain concrete is outlined together with the FCM model of the same crack.

From a modelling point of view the second assumption makes the application of the FCM in FEM formulations particularly simple since the crack can be modelled with so-called interface elements

(1) In the original formulation of the FCM, the process zone and the fictitious crack are synonyms; here however two different mechanisms are associated with the fictitious crack: micro-cracking in the process zone and aggregate interlock (along with fibre bridging - in the case of tension softening SFRC).

(2) According to linear elastic analysis of cracks infinitely large stresses – stress singularities – always exist at sharp crack tips. In linear elastic fracture mechanics these singularities are characterized through so-called stress intensity factors which depend only on geometry and loading. Crack propagation is assumed to take place when the stress intensity factor reaches a critical value.

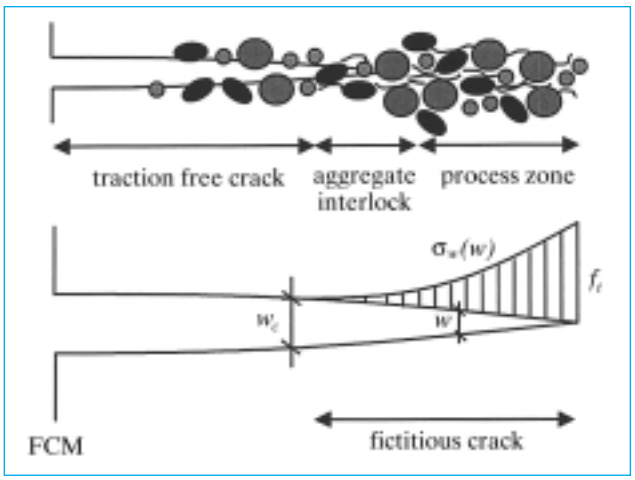

Fig. 2 - Outline of a concrete crack and the essential features: the process zone, aggregate interlock and traction free crack together with the FCM. (After [13]).

containing information about the stress-crack opening relationship $\sigma_w(w)$.

The third assumption means that the basic fracture property is the stress-crack opening relation $\sigma_w(w)$. It is usually assumed that this function is a monotonically decreasing function, indicating softening behaviour. It is furthermore assumed that:

$$\sigma_w(0) = f_t \tag{1}$$

where f_t is the tensile strength. Additionally, a characteristic crack opening w_c is defined by:

$$\sigma_w(w_c) = 0 \tag{2}$$

see Fig. 2. Assuming that the shape of the stress-crack opening relationship is more or less independent of material type, the stress-crack opening relation can be defined in terms of the area under the curve and since no energy dissipation is assumed to take place in the crack tip, this area can be equated with the fracture energy, G_F:

$$G_F = \int_0^{w_c} \sigma_w(w)dw \tag{3}$$

From a modelling point of view, any constitutive continuum modelling can be chosen in the bulk material. Often a simple linear elastic modelling is chosen. Introducing the Young's modulus E, the characteristic length l_{ch} can be defined:

$$l_{ch} = \frac{EG_F}{f_t^2} \tag{4}$$

The characteristic length can be interpreted as the ratio between fracture energy per crack area and elastic energy per volume for a given material. The characteristic length can be used to characterize the brittleness of a given material but can also be used to define a dimensionless structural brittleness number B by taking the ratio of a representative structural dimension L to the characteristic length of the material:

$$B = \frac{Lf_t^2}{EG_F} \tag{5}$$

2.3 Fracture mechanics for SFRC

The stress-crack opening relationship lends itself in a very natural way to the description of fracture of short fibre reinforced materials with SFRC behaviour. In fact the fictitious crack approach was suggested by Hillerborg for use in the description of formation of cracks in fibre reinforced concrete [11] introducing an approach where the stress-crack opening relationship now describes the stresses carried by fibres across a tensile crack in the composite material as function of the crack opening. Later this approach has been taken by numerous authors in attempts to describe the crack bridging ability of fibres – the so-called fibre bridging – in different brittle matrix composite systems, [4, 15-18]. The fictitious crack in SFRC materials now represents the process zone, aggregate interlock as well as fibre bridging, see Fig. 3.

Though similar in many aspects, in others the FCM approach for crack initiation, propagation and opening in SFRC differs significantly from the FCM approach to concrete fracture. Since the fibre bridging is closely related to the fibres debonding and pulling out, and since the fibres often have a length that is not small compared to crack openings accepted in real structures, from a practical point of view, the parameter w_c is not relevant. This implies that in analysis of SFRC materials, G_F defined by Equation (3) loses its significance from a practical, structural point of view. Furthermore, the stress-crack opening curve shape depends on the type and amount of fibre used, and the shape of the curve influences the structural behaviour. Thus, the actual variation of the function $\sigma_w(w)$ in the range of acceptable crack openings – *e.g.* 0-1.5 mm – becomes more important than G_F.

Finally, it is very important to realize that in many practical applications the fibres are not randomly distrib-

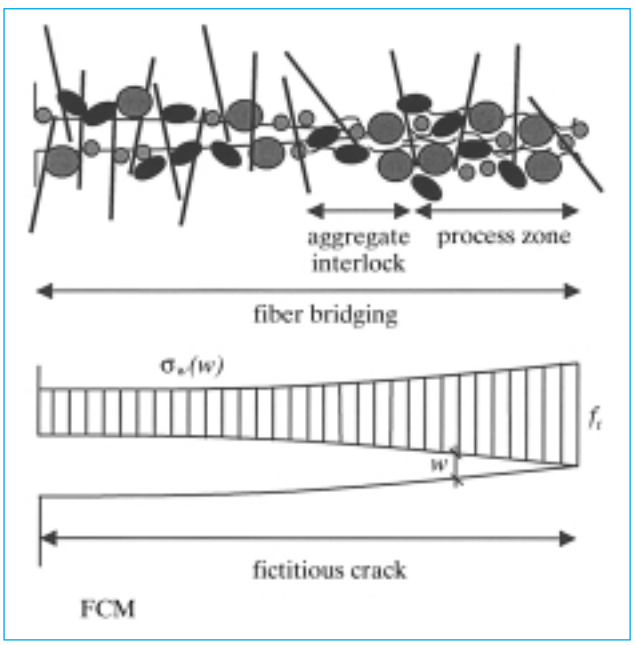

Fig. 3 - A crack in SFRC and the essential features: zone with fibre bridging, the process zone and aggregate interlock together with the FCM.

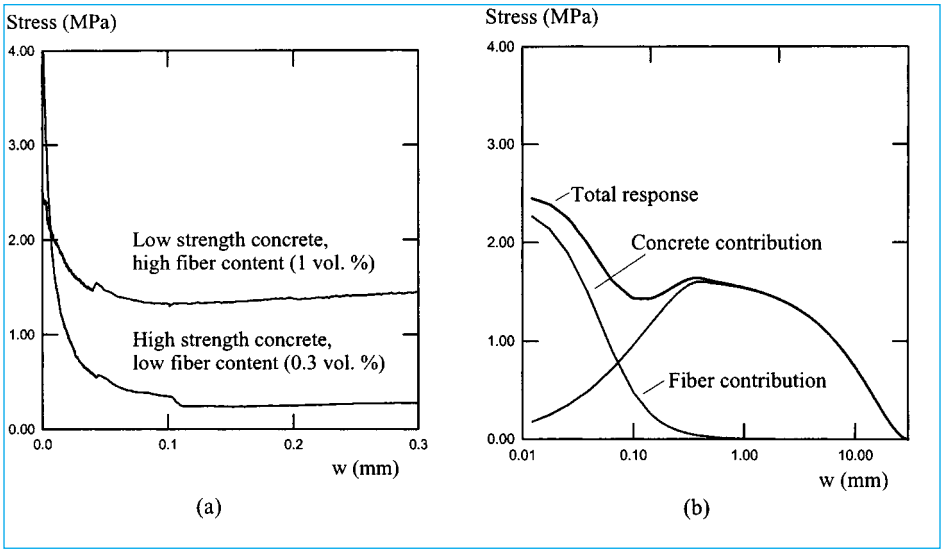

Fig. 4 - Typical stress-crack opening relationships (a) obtained from experimental measurements on steel fibre reinforced concrete containing 0.3 and 1 vol.% of hooked end steel fibres in high and low strength concrete, respectively. In (b) is shown a conceptual theoretical modelling of the relationship, following [18], showing the concrete and the fibre contributions. (Note the logarithmic length scale).

uted. As a consequence, the stress-crack opening relationship of SFRC materials cannot be considered an isotropic property, *i.e.* the relationship depends on the direction of cracking relative to the fibre orientation. Often the fibres are oriented during the casting process. In surface layers fibres are to a certain extent oriented parallel to the external surface (the so-called wall effect) and sometimes the thickness of the structural member is of the same order of magnitude as the fibre length (*e.g.* pavements), which causes fibres to be oriented throughout the thickness of the structural member.

3. STRESS-CRACK OPENING RELATIONSHIPS FOR DESIGN

3.1 General

Experimental determination of the stress-crack opening relationship can be done in a fundamental way using the uniaxial tension test [3, 29, 30]. As mentioned in the previous section, the shape of the stress-crack opening relationship depends heavily upon the type and amount of fibre used. The relationship can be divided into a concrete contribution and a fibre contribution. The concrete contribution is the softening stress-crack opening relationship for the unreinforced concrete, while the fibre contribution consists of a steeply ascending part followed by a slowly descending or softening part. The first part of the resulting relationship – up to crack openings of about 0.1-0.2 mm – is a result of the competing concrete and fibre contribution, while the relationship for larger crack openings is due mainly to the fibre contribution. The resulting total response consists of first a descending part, then a slowly ascending and finally a descending or softening part, see Fig. 4.

For design purposes, simplified versions of the stress-crack opening relations need to be defined.

3.2 Multi-linear relationship

Very realistic representations of measured stress-crack opening relationships can be obtained with a multi-linear function:

$$\sigma_w = \sigma_i - \alpha_i w, \quad w_{i-1} < w \le w_i = \frac{\sigma_{i+1} - \sigma_i}{\alpha_{i+1} - \alpha_i}, \qquad (6)$$
$$w_0 = 0, \quad \sigma_1 = f_t \quad \alpha_1 > 0$$

The multi-linear stress-crack opening relationship is illustrated in Fig. 5. As indicated in Fig. 5 the slopes α_i of the different linear sections of the multi-linear function can be positive and negative. It is assumed, however, that the tensile strength is never reached again after softening has been initiated.

3.3 Bi-linear relationship

For many SFRC materials a bi-linear relationship provides a reasonable representation of the measured behaviour, compare with Fig. 4:

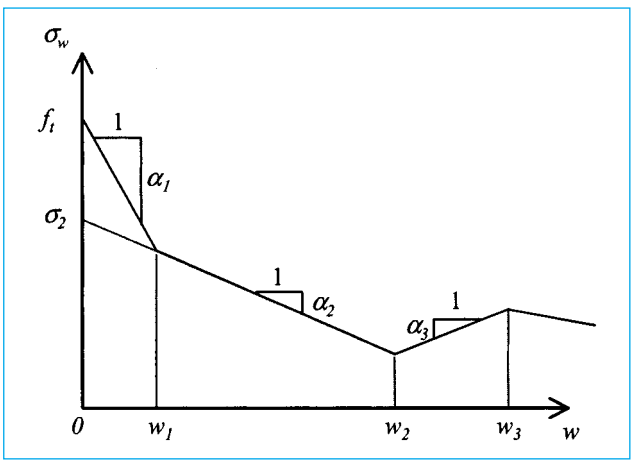

Fig. 5 - Illustration of the multi-linear stress-crack opening relationship. In the figure α_1 and α_2 are positive, α_3 is negative.

$$\sigma_w(w)=\begin{cases}\sigma_1-\alpha_1 w \ \text{ for} \\ 0\le w\le w_1=\dfrac{\sigma_2-\sigma_1}{\alpha_2-\alpha_1} \ \ \alpha_1>0 \ \ \sigma_1=f_t \\ \sigma_2-\alpha_2 w \ \text{ for } \ w_1<w\le w_c=\dfrac{\sigma_2}{\alpha_2} \ \ \alpha_2>0\end{cases} \tag{7}$$

In this approach a total of four material parameters are required to describe the stress-crack opening relationship.

The bi-linear stress-crack opening relationship is illustrated in Fig. 6. In the limiting case where α_1 becomes very large compared to α_2, the bi-linear relationship becomes what is called a drop-linear relationship, reducing the number of parameters to three.

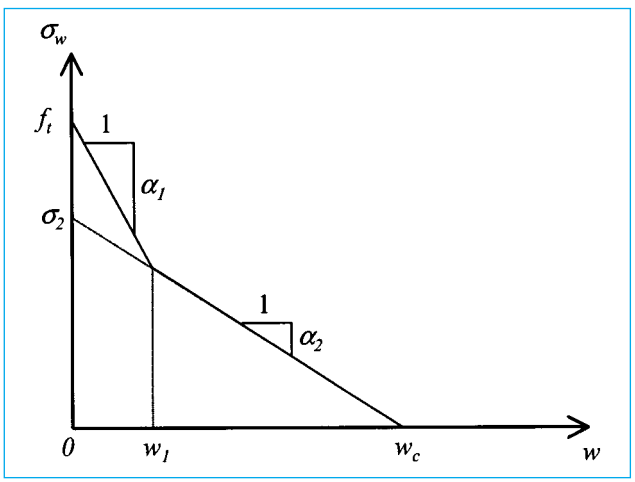

Fig. 6 - Illustration of the bi-linear stress-crack opening relationship.

3.4 Drop-constant relationship

An even more simple representation which has obvious advantages from a design point of view is the so-called drop-constant relationship:

$$\sigma_w(w)=\begin{cases}f_t \ \text{ for } \ w=0 \\ \sigma_y \ \text{ for } \ w<w_{\max}\end{cases} \tag{8}$$

defining a *residual strength* σ_y which characterizes the relationship up to a certain maximum crack opening w_{max}.

In this approach a total of two (or three – counting w_{max}) material parameters are required to describe the stress-crack opening relationship.

The drop-constant stress-crack opening relationship is illustrated in Fig. 7.

3.5 Free-form relationship

In previous work, [32], it has been shown that the σ-w relationship of the form (9) can be used to model a large variety of SFRC materials using empirical variations of the parameters w^* (reference crack width) and p (shape parameter):

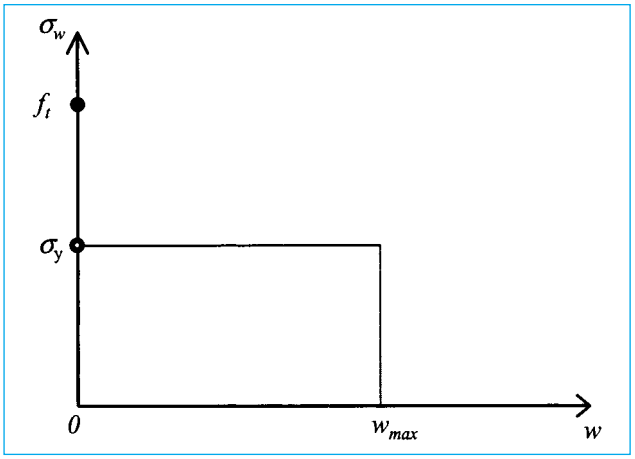

Fig. 7 - Illustration of the drop-constant stress-crack opening relationship.

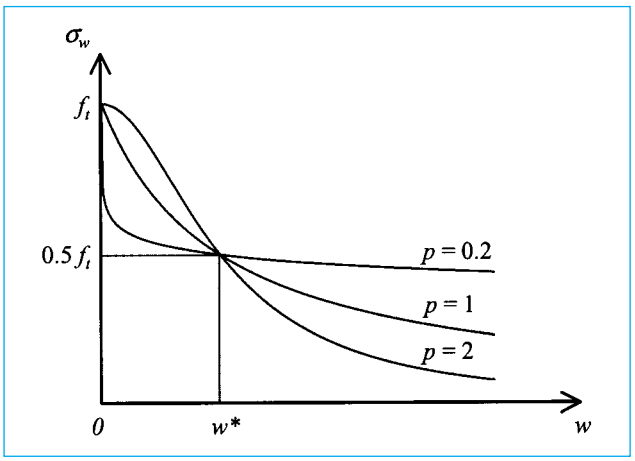

Fig. 8 - Illustration of the free-form stress-crack opening relationship and the influence of the shape parameter p for a fixed value of w^*.

$$\sigma_w(w)=\frac{f_t}{1+\left(\dfrac{w}{w^*}\right)^p} \tag{9}$$

Again, two material parameters are associated with the model. The free-form stress-crack opening relationship is illustrated in Fig. 8.

3.6 Characteristic values and safety factors

The analysis of SFRC structures based on the material parameters described above should be carried out according to the principles known from standard concrete structural analysis and design.

Thus, based on materials testing, an average and a characteristic response should be identified, see below. Analysis in the serviceability limit state should be based on assumed or measured characteristic values, while analysis and design in the ultimate limit state should be based on characteristic values modified with safety factors. At this stage only limited experience has been gained with struc-

tural design based on fracture mechanical principles. Safety factors should be code related. It is outside the scope of the present document to give specific values.

In design of minimum reinforcement and design for crack widths in traditional reinforced concrete structures, the under-estimation of tensile strength, f_t can lead to non-conservative results regarding safety and crack openings. Similarly in SFRC structures, both the upper and lower characteristic value of f_t should be considered depending on which results in the more critical situation. The lower characteristic value of $\sigma_w(w)$ for $w > 0$ will always result in the more critical situation.

3.7 Experimental determination and verification

For experimental determination of the stress-crack opening relationship it is useful to distinguish between tests aiming for direct determination of the relationship and methods aiming for verification of a simplified version of the relationship used in design. In this context it should be noted that no generally accepted standards for either direct determination or verification of the stress-crack opening relationship exist at this point in time.

Methods for direct determination of the stress-crack opening relationship are typically based on a uniaxial tension testing configuration.

A standard for uniaxial tension testing method for SFRC (as well as other types of FRCC) has been proposed in [3]. Here a method for the direct determination of the characteristic stress-crack opening curve $\sigma_{w,k}(w)$ from the average curve $\bar{\sigma}_w(w)$ is described. Care must be taken to obtain a fibre orientation in the test specimen that is representative of the orientation in the structural application, see Section 2.3. The uniaxial tension test method is not suitable for determination of the tensile strength f_t. It is assumed that information about the characteristic and design tensile strengths, $f_{t,k}$ and $f_{t,d}$ is obtained independently, through codes or standard testing methods intended for plain concrete. The principle is illustrated in Fig. 9.

A stress-crack opening curve for use in serviceability limit state analysis may be obtained from the uniaxial testing result and information about tensile strength using curve fitting of any of the suggested material models, Equations (6) to (9) to the characteristic stress-crack opening relationship. It is recommended that the fitted analytical relationship always lies below the characteristic curve. Furthermore, the fitted stress-crack opening relationship should always be overall descending, *i.e.* the characteristic tensile strength should never be reached again.

The design stress-crack opening relationship $\sigma_{w,d}(w)$ for use in ultimate limit state analysis is obtained from the characteristic relationship based on the lower characteristic tensile strength by division with a safety factor.

Experimental verification of assumed stress-crack opening curves can be carried out through a direct comparison with uniaxial test data. Stang and Olesen [34] suggested to carry out bending tests with a notched beam, *e.g.* according to [1], and to compare the test

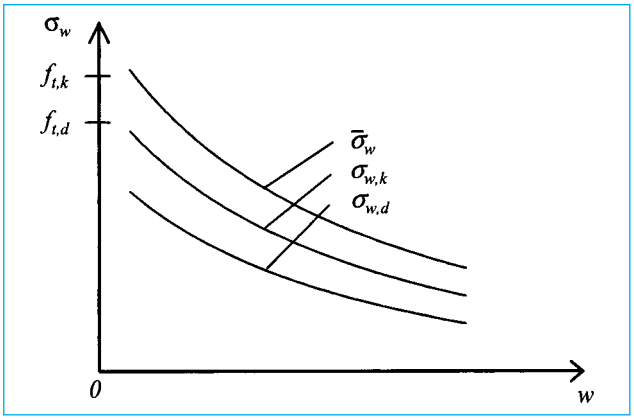

Fig. 9 – Illustration of average, $\bar{\sigma}_w(w)$, characteristic, $\sigma_{w,k}(w)$, and design, $\sigma_{w,d}(w)$, stress-crack opening relationships. The average and the characteristic curves are based on testing experience. The design curve is related to the characteristic curve through a safety factor. The characteristic tensile strength $f_{t,k}$ and the design value $f_{t,d}$ are code related properties or properties obtained from independent testing.

results with pre-calculated, expected responses. The expected response can be calculated for any of the suggested material models, Equations (6) to (9). This method is still under investigation.

It should also be noted that much work has been carried out in order to set up methods of inverse analysis to derive the stress-crack opening relationship from bending tests, [14, 23]. Some difficulties with this type of approach were pointed out in [33].

4. CROSS-SECTIONAL ANALYSIS FOR FLEXURE AND AXIAL FORCES

4.1 General - non-linear hinge

A cross-sectional analysis of the cracked section of *e.g.* a beam, a pipe or a slab can be carried out by describing the cracked section as a non-linear hinge.

The idea of the non-linear hinge model is to analyze separately the section of the structural element where the crack is formed and assume that the rest of the structure behaves in a linear elastic fashion. In order for the non-linear hinge to connect to the rest of the structure, the end faces of the non-linear hinge are assumed to remain plane and to be loaded with the generalized stresses in the element.

The principle of the analysis in the case of a structural element subjected to a combination of flexure and axial force is shown in Fig. 10. The structural element is divided into a non-linear hinge of length s where the main non-linear behaviour due to cracking is concentrated and into other parts that are considered to behave elastically.

The non-linear analysis for fictitious crack propagation and associated load carrying capacity is carried out only for the non-linear hinge loaded with the generalized stresses, in this case a axial force N and a moment M.

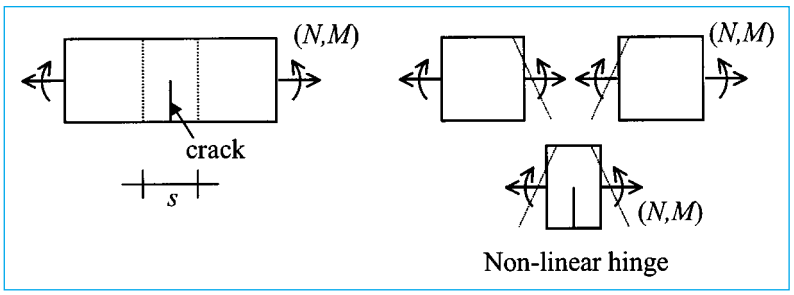

Fig. 10 - The principle of the non-linear hinge analysis in the case of a structural element subjected to a combination of flexure and axial force (left). As shown in the right hand side, the element is divided into a middle section of width s containing the crack – the so-called non-linear hinge – and the rest of the element which is assumed to behave elastically. The non-linear analysis for crack propagation and associated load carrying capacity is carried out only for the non-linear hinge.

4.2 Geometrical assumptions

A number of different solutions for rectangular cross-section can be found in the literature based on different assumptions regarding kinematic and constitutive conditions. An overview of different constitutive relations in terms of the stress-crack opening relation governing the traction on the fictitious crack as function of the crack opening can be found above.

Different kinematic assumptions applied in various models are shown schematically in Fig. 11 and can be described in the following way:

- The fictitious crack surfaces remain plane and the crack opening angle equates the overall angular deformation of the non-linear hinge, [28], (a) in Fig. 11.
- The fictitious crack surfaces remain plane and the crack opening angle equates the overall angular deformation of the non-linear hinge. Furthermore, the overall curvature of the non-linear hinge, the curvature of the cracked part and the curvature of the elastic part are linked based on an assumption of parabolic variation of the curvature [6, 7], (a) in Fig. 11.
- The fictitious crack surfaces do not remain plane, the deformation is governed by the stress-crack opening relationship, the crack length and the overall angular deformation of the non-linear hinge, see [35] for linear stress-crack opening relationship and [26] for a bi-linear stress-crack opening relationship and the drop-linear relationship, (b) in Fig. 11.

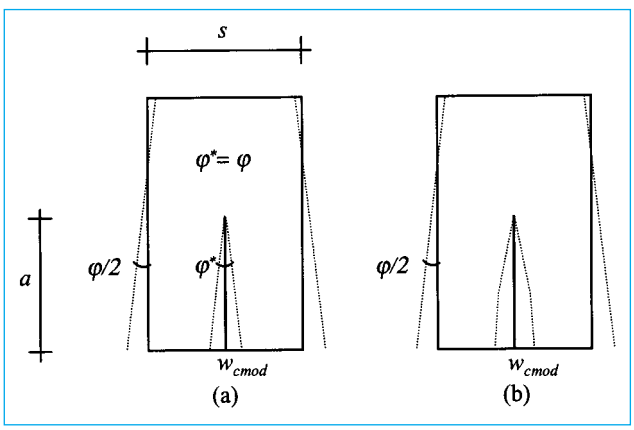

Fig. 11 – Different kinematic assumptions applied in various non-linear hinge models. In (a) the fictitious crack surfaces remain plane and the crack opening angle equates the overall angular deformation. In (b) the fictitious crack surfaces do not remain plane, the deformation is governed by the stress-crack opening relationship.

In all cases the average curvature of the non-linear hinge, κ_m is given by:

$$\kappa_m = \frac{\varphi}{s} \tag{10}$$

In the first two approaches, the crack mouth opening displacement w_{cmod} (the crack opening at the bottom of the non-linear hinge) follows directly from the crack opening angle φ^* and the length of the fictitious crack, a:

$$w_{cmod} = \varphi^* a \tag{11}$$

while the crack mouth opening displacement in the third approach is determined from the stress-crack opening relationship, the overall curvature κ_m and the length of the fictitious crack.

4.3 Analysis for rectangular sections

The analysis according to the three different kinematic assumptions is presented below. In all cases the solutions can be generalized to cover T-sections, non-linear material behaviour in compression etc.

Simplified approach by Pedersen

The following analysis follows the analysis in [28]. The analysis allows for the application of any stress-crack opening relation using numerical integration to obtain the solution. The analysis takes into account combined axial force and moment on the cross section.

Consider a non-linear hinge with rectangular cross-section and depth h. The cross section is subjected to an external bending moment M per width and the axial force N per width of the element. As long as the tensile strength is not reached the element is assumed to behave linear elastically according to classic Bernouilli beam theory.

When the tensile strength is reached, it is assumed that a single crack is formed with a maximum tensile stress f_t at the crack tip. Fig. 12 shows the assumed distribution of stresses where the post-peak tensile stress is a function of the crack width given by the stress-crack opening relationship, $\sigma_w(w)$. Note that it is assumed that the compressive zone remains in the linear elastic range.

As indicated in Fig. 12 it is assumed that the crack has a linear profile (see also [19]), thus the crack opening angle φ^* is related to the crack mouth opening w_{cmod} and the length of the fictitious crack a as follows:

$$\varphi^* = \frac{w_{cmod}}{a} \tag{12}$$

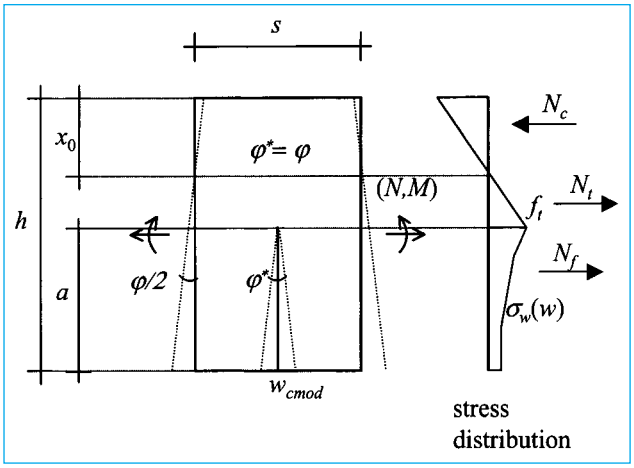

Fig. 12 - The analysis according to the simplified approach by Pedersen. The non-linear hinge subjected to axial force and moment is shown along with the assumed stress distribution and the resulting forces in the different regions.

Now, the distribution of normal stresses within the cracked zone is given by the stress-crack opening relationship, $\sigma_w(w)$ and the resulting force per width of the cracked zone and the bending moment per width of the cracked zone taken at the crack tip, N_f and M_f respectively, can be obtained by integrating:

$$N_f = \frac{1}{\varphi^*}\int_0^{w_{cmod}} \sigma_w(u)du \tag{13}$$

$$M_f = \frac{1}{(\varphi^*)^2}\int_0^{w_{cmod}} \sigma_w(u)udu \tag{14}$$

It is now required that the crack opening angle corresponds to the total angular deformation of the non-linear hinge. With the given assumptions the depth of the tensile zone, $h - x_0$, (see Fig. 12) in the non-linear hinge may now be related to the crack mouth opening by:

$$h - x_0 = \frac{1}{\varphi}\left(\frac{f_t}{E}s + w_{cmod}\right) \tag{15}$$

where s is the length of the non-linear hinge.

The resulting force per width of the elastic compression zone is denoted N_c and the resulting force per width of the elastic tensile zone is denoted N_t:

$$N_c = \frac{\varphi E x_0^2}{2s} \tag{16}$$

$$N_t = \frac{(f_t)^2 s}{2\varphi E} \tag{17}$$

Equation (16) describes how N_c is related to φ and x_0: $N_c(\varphi, x_0)$. Equation (17) describes how N_t is related to φ: $N_t(\varphi)$. Equation (13) describes how N_f is related to φ and w_{cmod}: $N_f(\varphi, w_{cmod})$.

Denoting the resulting axial force per width of the element N, for a given angular deformation φ, the equilibrium of the section is written in the following way in order to determine the position of the neutral axis:

$$N_t(\varphi) + N_f(\varphi, w_{cmod}) - N_c(\varphi, x_0) = N \tag{18}$$

The crack mouth opening w_{cmod} can be substituted from Equation (15):

$$N_t(\varphi) + N_f(\varphi, x_0) - N_c(\varphi, x_0) = N \tag{19}$$

Given φ and N the position of the neutral axis can be determined from Equation (19).

Now the moment M relative to the center line of the cross section can be determined. The moment is given by:

$$M = \left(\frac{h}{2} - \frac{x_0}{3}\right)N_c + \left(\frac{h}{6} + \frac{x_0}{3} - \frac{2a}{3}\right)N_t + \left(\frac{h}{2} - a\right)N_f + M_f \tag{20}$$

where a is determined by Equations (12) and (15). Thus the result of the calculation is corresponding values of angular deformation, axial force, and bending moment:

$$M = M(\varphi, N) \tag{21}$$

and the solution constitutes the characteristics of the non-linear hinge.

Furthermore, results are obtained for fictitious crack length a, crack mouth opening w_{cmod} and stresses.

The non-linear Equation (19) can be solved for x_0 using a simple numerical iteration technique, *e.g.* bisection. Furthermore, the involved integrations in Equations (13) and (14) can be carried out using a numerical integration scheme allowing for the use of any stress-crack opening relationship $\sigma_w(w)$.

Simplified approach by Casanova

Casanova and Rossi, [7], proposed a model which adopts the assumptions shown on Fig. 11 (a) with respect to the angle at the faces of the non-linear hinge and the crack opening angle. In the model it is assumed that the angle formed by the crack varies according to the crack mouth opening and the depth of the crack:

$$\varphi = \frac{w_{cmod}}{a} \tag{22}$$

The length s of the non-linear hinge in Casanova's model varies with the depth of the crack such that:

$$s = 2a \tag{23}$$

The final assumption is related to the internal kinematics of the hinge. Two curvatures are considered, the elastic curvature of the un-cracked part of the hinge, κ_1, and the curvature in the cracked zone, κ_2. The elastic curvature is given by:

$$\kappa_1 = \frac{12M}{Eh^3} \tag{24}$$

where M is the moment per unit width in the beam.

The curvature in the cracked zone is given by:

$$\kappa_2 = \frac{\varepsilon_c}{x_0} \tag{25}$$

where ε_c is the strain at the extreme fibre in compression, and x_0 is the depth of the neutral axis at the crack.

The depth of the neutral axis in the un-cracked (elastic) zone in Casanova's model is based on linear elasticity. Thus, although $\varphi = \varphi^*$, the neutral axis, and therefore the curvature, are different at the faces of the non-linear hinge and at the crack.

The curvature in the un-cracked and the cracked part of the hinge is linked to the average curvature κ_m (see Equation (10)) of the hinge by assuming a parabolic variation of the curvature along the non-linear hinge:

$$\kappa_m = \frac{2\kappa_1 + \kappa_2}{3} \tag{26}$$

Combining Equations (22) to (26) leads to the basic constitutive relationship of the model proposed in [7]:

$$w_{cmod} = 2\kappa_m a^2 = 2\left(\frac{2\kappa_1 + \kappa_2}{3}\right)a^2 \tag{27}$$

Equations (13) to (14) and (16) to (20) presented for Pedersen's model are directly applicable with Casanova's model when φ/s is replaced with κ_m. Again, the equilibrium equation (19) has to be solved by numerical iteration.

In the above a linear stress-strain relationship for the concrete in compression or in tension outside the cracked zone is adopted. In the general case where a non-linear stress-strain relationship for concrete in compression is chosen, a numerical integration over depth of the cross section can be carried out. This approach has been used by [20] to predict the response of fibre reinforced slab elements.

Explicit formulation by Olesen

It is possible to obtain a closed form solution for the non-linear hinge when using a multi-linear or bi-linear stress crack-opening relationship in combination with the kinematic assumption that the boundaries of the non-linear hinge remain plane while the fictitious crack plane deformation is governed by the stress-crack opening relationship as well as the overall angular deformation of the non-linear hinge and the length of the fictitious crack.

In particular a solution for the moment-rotation relationship in the case of zero axial force and a bi-linear stress-crack opening relationship was presented in [33]. The complete solution for the bi-linear stress-crack opening relationship including a non-zero axial force can be found in [26]. The derivation in the following follows [33] closely.

The non-linear hinge is modelled as incremental layers of springs that act without transferring shear between each other, see Fig. 13. The vertical boundaries of the hinge are assumed to remain straight during deformation and the total angular deformation of the non-linear hinge is again denoted φ.The associated longitudinal deformation of the springs is denoted $u(x)$ where x is a vertical co-ordinate, see Fig. 13. The average curvature of the non-linear hinge, κ_m, is given by Equation (10), while the mean longitudinal strain, $\varepsilon^*(x)$, is given by:

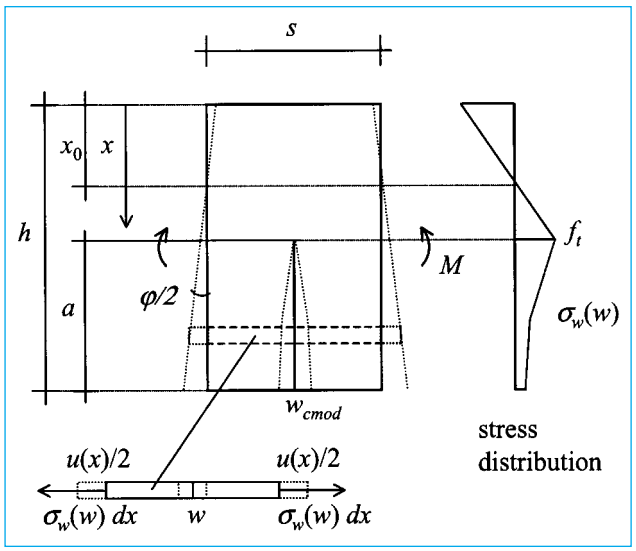

Fig. 13 - The modelling of the propagation of the fictitious crack through the non-linear hinge used in the explicit formulation. Below the non-linear hinge: illustration of an incremental horizontal layer of the band. To the right: the associated stress distribution.

$$\varepsilon^*(x) = \kappa_m(x - x_0) = \frac{u(x)}{s} \tag{28}$$

where x_0 is the co-ordinate of the neutral axis in the hinge. It is assumed that the hinge layers behave linear elastically as long as the tensile strength f_t is not reached. When the stress reaches f_t a fictitious crack is assumed to form with a stress-crack opening relationship σ_w which is a function of the crack opening w which in turn is a function of x. The deformation u of a layer may then be obtained from:

$$u(x) = \frac{\sigma_w(w(x))}{E}s + w(x) \tag{29}$$

Considering that the axial force is zero and that the stress-crack opening relation $\sigma_w(w)$ is the bi-linear function, Equation (7), four different stress distributions develop in the cross section as the fictitious crack grows. The different phases are shown in Fig. 14. The phases are governed by the parameters x_1 and x_2 given by the general expression:

$$x_i = x_0 + \frac{1}{\varphi}\left[\varsigma_i - w_i(\psi_i - 1)\right] \quad i = 1,2 \tag{30}$$

where

$$\varsigma_i = \frac{\sigma_i s}{E} \quad \psi_i = \frac{\alpha_i s}{E} \quad i = 1,2 \tag{31}$$

The following normalizations are introduced:

$$\mu = \frac{6}{f_t h^2 t}M, \quad \theta = \frac{hE}{2sf_t}\varphi, \quad \alpha = \frac{a}{h} \tag{32}$$

where a is the depth of the fictitious crack. The moment is normalized with the moment which causes the crack initiation while the angular deformation is normalized with the angular deformation at crack initiation. Given

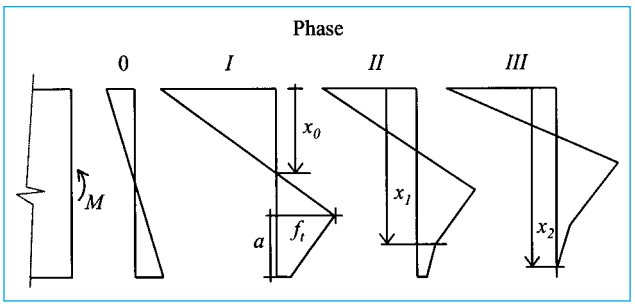

Fig. 14 - Definition of the four different phases of stress distribution experienced during crack propagation.

these normalizations the pre-crack elastic behaviour of the hinge is described by the relation $\mu = \theta$ with $0 \le \theta \le 1$. The complete solution in the three crack development phases is given below. For convenience the following properties *b* and *c* are introduced:

$$b = \frac{\sigma_2}{f_t} \tag{33}$$

$$c = \left(1-b\right)\left(1-\psi_1\right)/\left(\psi_2-\psi_1\right) \tag{34}$$

The analysis of the non-linear hinge is carried out with θ as the controlling parameter. Thus, the values of θ corresponding to phase transitions need to be known. Three different values are relevant, $\theta_{0\text{-}I}$, $\theta_{I\text{-}II}$ and $\theta_{II\text{-}III}$:

$$\theta_{0-I} = 1 \tag{35}$$

$$\theta_{I-II} = \frac{1}{2}\left(1-c+\sqrt{\left(1-c\right)^2+\frac{c^2}{\psi_1-1}}\right) \tag{36}$$

$$\theta_{II-III} = \frac{1}{2}\left(\frac{b}{\psi_2}+\sqrt{\frac{\left(1-b\right)^2}{\psi_1-\psi_2}+\frac{b^2}{\psi_2}}\right) \tag{37}$$

For phase *I* with $\theta_{0\text{-}I} \le \theta \le \theta_{I\text{-}II}$ the solution reads:

$$\alpha = 1-\psi_1-\sqrt{\left(1-\psi_1\right)\left(\frac{1}{\theta}-\psi_1\right)} \tag{38}$$

together with:

$$\mu = 4\left(1-3\alpha+3\alpha^2-\frac{\alpha^3}{1-\psi_1}\right)\theta-3+6\alpha \tag{39}$$

For phase *II* with $\theta_{I\text{-}II} \le \theta \le \theta_{II\text{-}III}$ the solution reads:

$$\alpha = 1-\psi_2-\frac{1-b}{2\theta}-\sqrt{\left(1-\psi_2\right)\left(\frac{\left(1-b\right)^2}{4\theta^2\left(\psi_1-\psi_2\right)}-\psi_2+\frac{b}{\theta}\right)} \tag{40}$$

together with:

$$\mu = 4\left(1-3\alpha+3\alpha^2-\frac{\alpha^3}{1-\psi_2}\right)\theta - 3+6\alpha-\frac{\left(1-b\right)\left(3\alpha^2-\left(\frac{c}{2\theta}\right)^2\right)}{1-\psi_2} \tag{41}$$

For phase *III* with $\theta_{II\text{-}III} \le \theta$ the solution reads:

$$\alpha = 1-\frac{1}{2\theta}\left(1+\sqrt{\frac{\left(1-b^2\right)}{\psi_1-\psi_2}+\frac{b^2}{\psi_2}}\right) \tag{42}$$

together with:

$$\mu = 4\left(1-3\alpha+3\alpha^2-\alpha^3\right)\theta-3+6\alpha-3\alpha^2+\frac{1}{4\theta^2}\left(1-\frac{b}{\psi_2}\right)\left(1-\frac{b}{\psi_2}+c\right)\left(1-\frac{\psi_1 c}{1-\psi_1}\right)+\left(\frac{c}{2\theta}\right)^2 \tag{43}$$

A closed form solution for w_{cmod} – the crack opening at the mouth of the crack – is obtained in [26]. In a compact form this can be written as:

$$w_{cmod} = \frac{sf_t\left(1-b_i+2\alpha\theta\right)}{E\left(1-\psi_i\right)} \tag{44}$$

where $(b_i,\Psi_i) = (1,\Psi_1)$ in phase *I*, (b,Ψ_2) in phase *II* and (0,0) in phase *III*.

With the simple drop-constant stress-crack opening relationship defined in Equation (8) involving the residual strength σ_y the $\mu(\theta)$ relationship reduces to the simple relationship, all in phase *I*, *i.e.* for $\theta > 1$:

$$\mu\left(\theta\right) = \gamma\left(3-2\sqrt{\frac{\gamma}{\theta}}\right) \tag{45}$$

with:

$$\gamma = \frac{\sigma_y}{f_t} \tag{46}$$

Furthermore, in this case the solution for w_{cmod} can be written as:

$$w_{cmod}\left(\theta\right) = \left(1-\gamma+2\alpha\theta\right)\frac{sf_t}{E} \tag{47}$$

with the normalized crack length given by:

$$\alpha = 1-\frac{1-\gamma}{2\theta}-\sqrt{\frac{\gamma}{\theta}} \tag{48}$$

Application of the non-linear hinge in structural analysis

Structural calculations of *e.g.* beams, [6, 7, 26, 28, 33-35], beams on elastic foundation [26] and pipes, [28], can be done by introducing a non-linear hinge in the structure, prescribing the angular deformation on the non-linear hinge, using the non-linear hinge solution to solve for the generalized stresses at the non-linear hinge, establish-

ing the linear elastic solution for the structure given the generalized stresses at the non-linear hinge and finally solving for the applied load and the total deformations. As an example, see section 5 and the appendix in case of a simply supported beam subjected to 3-point loading.

The length of the non-linear hinge s has to be considered a fitting parameter for the calculations. In general the optimal length will depend on the type of structural element. The hinge width s in a beam has previously been assessed ([28, 35]) using non-linear hinge models for plain as well as fibre reinforced concrete and it has been shown that $s = h/2$ is an adequate choice. Comparisons between the explicit model by Olesen, the simplified approach by [28] and the approach by [6] for the bi-linear stress-crack opening relationship show very similar results. Furthermore, all models compare favorably with a non-linear FEM analysis using the same bi-linear stress-crack opening relationship, see the appendix. This seems to indicate that, for a large number of stress-crack opening relationships, the simplified assumptions that the fictitious crack faces remain plane and that the deformation of the non-linear hinge is primarily due to the crack opening are reasonable.

4.4 Cross-section with conventional reinforcement

The models presented in Section 4.3 were aimed at predicting the behaviour of cross-sections reinforced only with fibres. In applications where conventional reinforcement is used with fibre concrete, additional assumptions related to the length of the non-linear hinge, the stress in the reinforcement at the crack, and the average curvature must be adopted.

In presence of reinforcement, SFRC members exhibit multiple cracking until reinforcement yielding. At that point, one crack generally governs the member behaviour due to the softening nature of fibre concrete. The assumptions must enable modelling the member response at small and moderate crack opening. At small crack opening under service loads, both the maximum crack width and the stress level limits in the reinforcement can have a significant importance (*e.g.* for durability purposes or for the fatigue of the reinforcement, [5]). In general, the ultimate load of a conventionally reinforced SFRC member corresponds to the situation when the conventional reinforcement yields. At this stage the fibre contribution to the load carrying capacity can be significant. In both cases it is therefore essential for the assumptions adopted to be realistic and representative of the actual behaviour.

Crack spacing

In direct tension and in flexure, the observed crack spacing in the presence of fibres is less than in identical members without fibres [9, 22, 36]. Although formulations have been proposed to determine crack spacing in the presence of fibres [22], further research has to be carried out in this area before a general formulation is available. However, attention should be drawn to the recent formulation of a so-called adaptive hinge model [25], which essentially is a non-linear hinge (section 4.3) that takes into account both the propagation of the fictitious crack and the de-bonding between re-bars and SFRC. The reason for calling the model the adaptive hinge is that the width of the hinge adapts itself to the de-bonded region on both sides of the bending crack. The model also provides information about crack opening and average curvature of the adaptive hinge. However, the model has not yet been experimentally verified. Therefore, until such information is available, crack spacing has to be evaluated based on reasonable assumptions. The formulation proposed in Eurocode 2, [10], for the average crack spacing and described in Test and Design Methods for Steel Fibre Reinforced Concrete. Recommendations for the σ–ε design method [2] gives an upper limit. Experimental evidence indicates that crack spacing in SFRC members smaller than the member depth is observed, both in flexure and in direct tension. It is therefore proposed to adopt the following assumptions for crack spacing, s_{rm}:

$$s_{rm} = 50 + 0.25 k_1 k_2 \frac{\phi}{\rho_r} \tag{49}$$

where ϕ is the bar diameter in mm whereas ρ_r, the effective reinforcement ratio, and parameters k_1 and k_2 are defined in [10].

The relationships presented in Section 4.3 for unreinforced concrete are applicable to members reinforced with conventional reinforcement. In this case the length of the non-linear hinge defined in Section 4.3 still applies to determine the response of the section. However in computing the deflection, [20] showed that more than one crack may govern the member behaviour and that a length equal to the member depth but not less than s or not less than the value given by Equation (49) should be used. They also showed that adopting the variable non-linear hinge length presented by [7] leads to reasonable results as compared to experimental results.

Reinforcement strains in the cracked region

Adopting Eurocode representation of the interaction between concrete and reinforcement allows us to consider reinforced SFRC member behaviour as a weighted average between the cracked and uncracked regions. Therefore the strain in conventional reinforcement in the cracked zone is given by:

$$\varepsilon_{s2} = \left(d - x_0\right)\kappa_2 \tag{50}$$

where d is the position of the reinforcement with respect to the compression face. This assumption is applicable with the simplified methods presented in Section 4.3.

Average curvature

The average curvature can be determined according to the recommendation [10], averaging the curvature at the crack and between cracks:

$$\kappa_m = (1-\zeta)\kappa_1 + \zeta\kappa_2 \tag{51}$$

with:

$$\zeta = 1-\beta_1\beta_2\left(\frac{\sigma_{sr}}{\sigma_{s2}}\right)^2 \tag{52}$$

where β_1 and β_2 are factors defined in [10], σ_{sr} is the stress in the reinforcement at the crack just after cracking whereas σ_{s2} is the current reinforcement stress at the crack. Curvatures κ_1 and κ_2 are computed in the uncracked and cracked regions respectively, using an iterative procedure, [20].

Alternatively, Equation (26) proposed in [7] for SFRC members only, can also be adopted to represent the average curvature over the non-linear hinge for members containing conventional reinforcement. This approach was used by [21] and showed good agreement with experimental results.

4.5 Limit states

Serviceability limit state

The serviceability limit state defines a maximum crack opening depending on the exposure class of the construction. Limiting crack openings are suggested in [2]. Both the case of steel fibre reinforced concrete with and without conventional reinforcement are covered. Code values may be adopted. Crack openings follow directly for the cross-sectional analysis described above.

Ultimate limit state

In case of cross sections without conventional reinforcement the ultimate limit state in bending is determined simply by the ultimate load carrying capacity calculated according to the above-mentioned methods.

In the case of under-reinforced cross-section, the ultimate load carrying capacity is usually reached at onset of reinforcement yielding. Beyond that point, the member exhibits a softening that is governed by the amount of reinforcement and the fibre concrete properties. At yielding of the reinforcement the concrete in compression can be first assumed to behave linear elastically which enables the use of the methods presented in Section 4.3. The maximum stress level in the concrete can then be checked. If the assumption is shown to be appropriate, the ultimate strength of the cross section determined with the methods presented above is adequate. In cases where the assumption of a linear behaviour in compression is not valid, the non-linearity of the concrete in compression should be taken into account as specified by codes for normal reinforced concrete members.

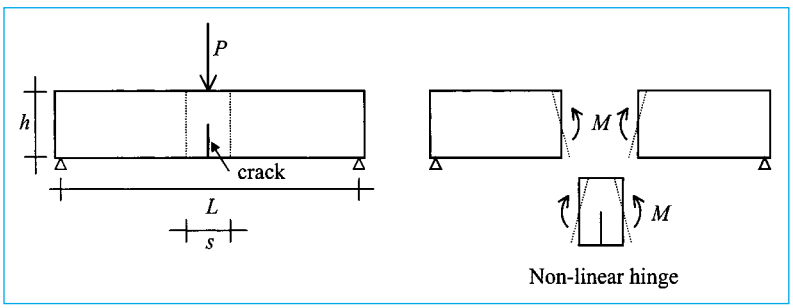

Fig. 15 - The principle of the non-linear hinge analysis in the case of a beam with rectangular cross-section, no conventional reinforcement, subjected to three point bending. The beam geometry and loading is shown on the left hand side. On the right hand side it is shown how the beam is divided into a middle section of width *s* containing the non-linear hinge and the rest of the beam which is assumed to behave elastically.

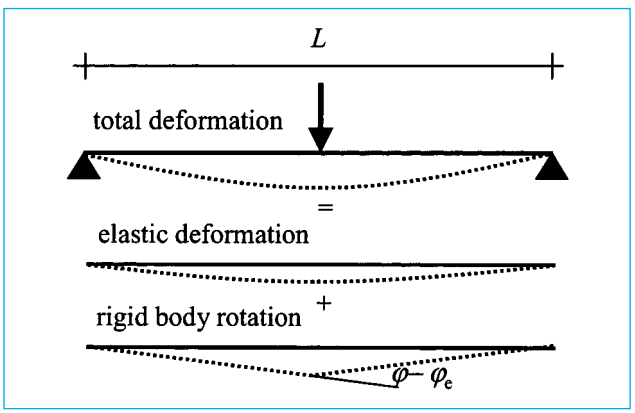

Fig. 16 - The principle of the superposition of elastic and cracking related deformation. The elastic deformation is calculated according to classical beam theory while the cracking related deformation is calculated from the deformation of the non-linear hinge, assuming that the rest of the beam rotates as stiff bodies.

5. BEAM ANALYSIS: LOAD-DEFLECTION BEHAVIOR

In this section the non-linear hinge is introduced in a simple beam without conventional reinforcement, loaded in three point bending and experiencing failure in bending, see Fig. 15.

Consider a beam with rectangular cross-section with depth h, width t and span L. The deflection u is calculated as a sum of two terms:

$$u = u_e + u_c \tag{53}$$

the elastic u_e and the cracking u_c related part of the deflection. This superposition of deformations is illustrated in Fig. 16.

According to classical beam theory u_e is related to the load P and the beam span L as follows:

$$u_e = \frac{PL^3}{48EI} \tag{54}$$

where E is Young's modulus of the SFRC-material and I is the moment of inertia of the cross section. The cracking related part of the deflection u_c is calculated modelling the crack as a generalized plastic hinge as shown above. In the calculation of this part the two halves of the beam are both assumed to be rigid and rotate an

angle ϕ:

$$\phi = \frac{\varphi - \varphi_e}{2} \tag{55}$$

where φ_e is the angular deformation of the non-linear hinge at the onset of cracking given by:

$$\varphi_e = \frac{12sM}{Eth^3} \tag{56}$$

while φ is the total angular deformation of the non-linear hinge prescribed in the cross-sectional analysis. The deflection due to the rigid-body rotation ϕ may be written in the form:

$$u_c = \phi \frac{L}{2} \tag{57}$$

In the elastic case the deflection is given by $u = u_e$. When a crack has developed the deflection is given by $u = u_e + u_c$. P is related to L and M by:

$$P = 4\frac{M(\varphi)}{L} \tag{58}$$

In this case the elastic deflection can be obtained from Equations (54) and (58).

The entire load deflection diagram for a beam in three point bending can be determined by prescribing angular deformations $\varphi > \varphi_{crack}$ of the non-linear hinge, calculating the load on the beam from Equation (58) and the two parts of the deformation from Equations (54) and (57). It follows that the load which initiates cracking P_{crack} is given by:

$$P_{crack} = f_t \frac{2h^2 t}{3L} \tag{59}$$

In Equation (58) any of the moment-rotation relationships described above can be applied. Furthermore, it was shown in [34] how the above analysis can be extended to cover the case of a beam with a notch.

Alternative approaches based on integration of the curvature along the length of the beam can be adopted, [20].

6. SHEAR CAPACITY: ULTIMATE LIMIT STATE

The shear capacity of FRC beams with conventional longitudinal reinforcing bars has been analyzed extensively in the literature [7] by considering the failure to occur due to crack propagation along known planes. Only such cases will be considered in this section since there is no generally accepted method for the determination of the shear capacity of FRC elements without conventional reinforcement. The approach of [7] to calculate the contribution from the fibres is described in the following.

Following Eurocode 2, [10], the ultimate shear load carrying capacity V_{Rd3} is taken to be the sum of the contributions of the member without shear reinforcement $V_{c,d}$, of the stirrups and/or inclined bars, $V_{w,d}$, and the steel fibres $V_{f,d}$:

$$V_{Rd3} = V_{c,d} + V_{w,d} + V_{f,d} \tag{60}$$

The contributions of the member without shear reinforcement and the stirrups and/or inclined bars can be calculated according to Eurocode 2. See also [2].

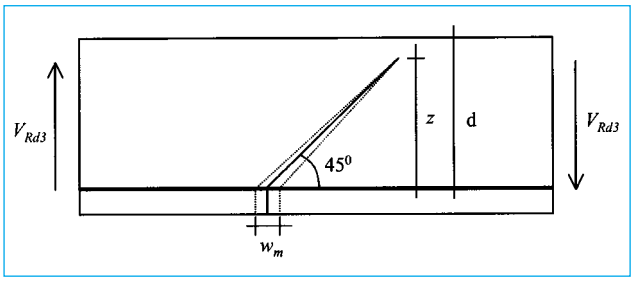

Fig. 17 - Assumed crack geometry in a beam with conventional, longitudinal reinforcement loaded to the ultimate shear loading capacity, V_{Rd3}. The crack is assumed to extend under 45°, and the crack opening at the re-bar is limited to w_m.

Considering a rectangular cross-section with width b, effective depth d (distance from the top of the beam to the reinforcing bars) and inner lever arm $z = 0.9d$, see Fig. 17, the fibre contribution $V_{f,d}$ is calculated from the design stress-crack opening relationship $\sigma_{w,d}(w)$ in the following way:

$$V_{f,d} = bz\bar{\sigma}_{p,d}(w_m) \tag{61}$$

with:

$$\bar{\sigma}_{p,d}(w_m) = \frac{1}{w_m}\int_0^{w_m} \sigma_{w,d}(u)du \tag{62}$$

The quantity $\bar{\sigma}_{p,d}(w_m)$ is called the mean design residual stress at the crack width w_m and represents the mean value of the post-cracking stress between zero and w_m.

A definition of w_m is necessary to quantify the ultimate load-carrying capacity of the beam failing in shear. Experimental studies carried out with different geometries of steel FRC beams, reinforced with conventional longitudinal re-bars, have analyzed the onset of inclined cracks and the formation of concrete struts in compression [6]. According to the results, the spacing of these cracks is roughly equal to the inner lever arm of the beam and the ultimate crack opening is proportional to the height of the beam. Since the crack opening is controlled by the longitudinal reinforcement, it is proposed that the maximum crack opening be taken as:

$$w_m = \varepsilon_s z \tag{63}$$

where ε_s is the strain of the longitudinal reinforcement.

Since $V_{f,d}$ typically decreases with an increase in the maximum crack opening, the fibre contribution should be determined for a maximum allowable crack width. If the maximum strain in the longitudinal steel re-bar is taken to be 1%, then w_m should be taken as $0.009d$.

In order to obtain an equivalence relationship between conventional transverse reinforcement and

fibres, we equate the contribution of $V_{w,d}$ to $V_{f,d}$ given in Equation (61) to obtain an equivalent mean design residual stress, $\bar{\sigma}^*_{p,d}(w_m)$:

$$\bar{\sigma}^*_{p,d}(w_m) = \frac{V_{w,d}}{bz} \tag{64}$$

This implies that the equivalent mean residual stress of $\bar{\sigma}^*_{p,d}(w_m)$ would yield the same load-carrying capacity as stirrups and/or inclined bars giving rise to $V_{w,d}$.

Furthermore, the equivalence in Equation (64) can be used to extend the definition of the minimum shear stirrup reinforcement given in the Eurocode 2 by:

$$\bar{\sigma}^*_{p,d} + \rho_t f_{y,d} \geq 0.02 f_{c,d} \tag{65}$$

where $f_{c,d}$ is the design compressive strength of the concrete, $f_{y,d}$ is the design yield strength of the stirrups and ρ_t is the area of stirrup reinforcement per unit length.

7. CRACK WIDTHS IN SLABS ON GRADE UNDER RESTRAINED SHRINKAGE AND TEMPERATURE MOVEMENT

Slabs on grade under restrained shrinkage and temperature movement is an important field of application for SFRC. The present section presents an analysis for the crack opening at crack formation in such structures. Simple design formulae based on the drop-constant stress-crack opening relationship Equation (8) are presented but other more complicated formulae can readily be applied. The present example follows closely [27].

An infinitely long slab of thickness h and unit width, cast onto a sub-base of *e.g.* graded gravel, is considered. The in-plane slab deformations are assumed to be governed only by shear stresses acting on the interface between the slab and the sub-base. Since the slab is infinitely long it will be completely restricted against longitudinal deformations. Thus, shrinkage or thermal strains developing in the slab will give rise to constant normal stresses throughout the length of the slab, assuming that the shrinkage and the thermal strains are homogeneous over the thickness. The normal stresses are assumed to be constant over the cross-section of the slab.

If the imposed strain – shrinkage or thermal contraction or a combination of both – attains such a value that the normal stress equals the tensile strength f_t of the slab material, then a crack is initiated. The objective of this example is to determine the crack opening as a function of the parameters in the drop-constant stress-crack opening relationship.

Fig. 18 shows the slab together with the stress distribution in the slab after it has cracked. The shear reaction acting on the bottom face of the slab against the longitudinal deformation of the slab, $u(x)$, is modeled as a two-parameter linear function:

$$|\tau(x)| = \tau_0 + \xi |u(x)| \tag{66}$$

where τ_0 and ξ are constants describing cohesion and hardening on the slab-sub base interface, respectively. The shear reaction always acts in the opposite direction of $u(x)$. The normal stress σ is given by:

$$\sigma = f_t + E\frac{du}{dx} \tag{67}$$

where E is the stiffness of the slab material. The differential equation governing the behaviour after crack initiation is readily established and reads as follows for the part of the slab to the left of the crack:

$$\frac{d^2u}{dx^2} = -\frac{|\tau|}{Eh} \tag{68}$$

Since all deformations are negative, Equations (66) and (68) may be combined to furnish:

$$\frac{d^2u}{dx^2} - \frac{\xi}{Eh}u = -\frac{\tau_0}{Eh}, \quad u < 0 \tag{69}$$

With the boundary conditions $u(0) = 0$ and $\sigma(0) = f_t$ the solution to this equation may be written as:

$$u(x) = -\frac{\tau_0}{\xi}\left(\cosh(\lambda x) - 1\right), \quad \lambda^2 = \frac{\xi}{Eh} \tag{70}$$

The state of stress in the slab is disturbed by the presence of the crack a distance l to either side of the crack. This length is unknown and depends on the opening of the crack, w, and a relation may be established by equating w to twice the displacement of the slab in $x = l$:

$$w = -2u(l) \Rightarrow \sinh(\lambda l) = \sqrt{\left(1 + \frac{w\xi}{2\tau_0}\right)^2 - 1} \tag{71}$$

We may now calculate the stress in the slab at the crack as a function of the crack opening.

Introducing Equation (70) into (67) and evaluating at $x = l$ we arrive at:

$$\frac{\sigma(l)}{f_t} = 1 - \frac{E}{f_t}\sqrt{\frac{w}{2}\left(\frac{2\tau_0}{Eh} + \frac{\xi}{Eh}\frac{w}{2}\right)} \tag{72}$$

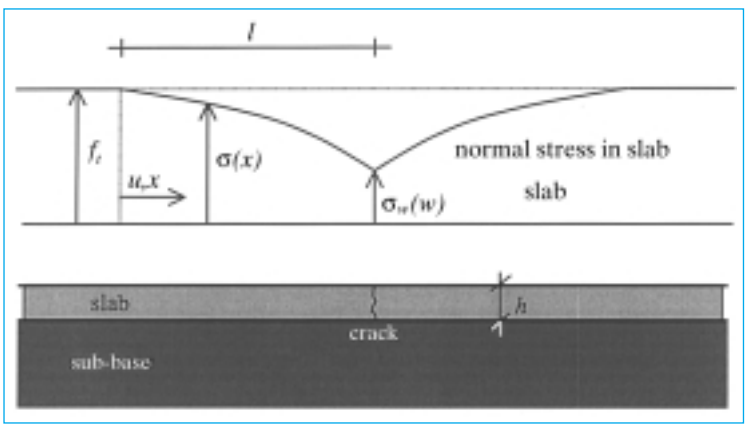

Fig. 18 – The stress distribution in an infinitely long, cracked slab restricted by shear stresses acting on the interface between slab and sub-base.

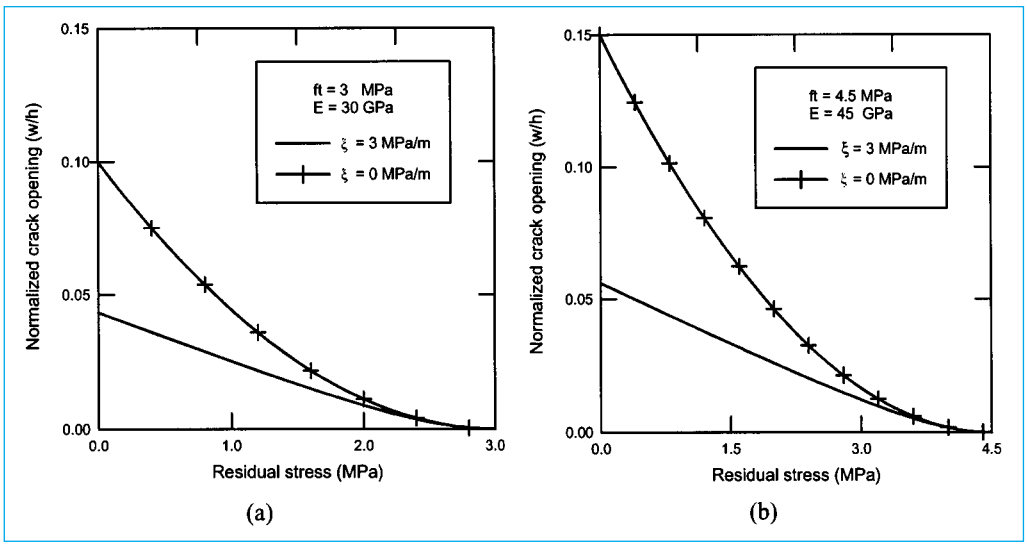

Fig. 19 - Crack opening divided by thickness of slab versus residual strength for two different strength levels, (a) f_t = 3 MPa, (b) f_t = 4.5 MPa. Applied parameter values: h = 0.12 m, τ_0 = 0.003 MPa, ξ = 0 and 3 MPa/m.

This equation denotes the equilibrium path, and it states the necessary stress to act on the crack surface in order to ensure equilibrium of the slab at a certain crack opening w. The stress-crack opening relationship for the slab material is a function of w and is written as $\sigma_w(w)$. Thus, the crack opening which ensures equilibrium is established by the equation:

$$\sigma(l) = \sigma_w(w) \tag{73}$$

This equation represents the general solution to the problem and is valid for any stress-crack opening relationship. Introducing the drop-constant stress-crack opening relationship Equation (8), the following expressions for the equilibrium crack opening may be deduced:

$$\frac{w}{h} = \begin{cases} 2\dfrac{\tau_0}{\xi h}\left(\sqrt{1+\dfrac{\xi h}{E}\left(\dfrac{f_t-\sigma_y}{\tau_0}\right)^2}-1\right) & \text{for } \xi \neq 0 \\ \dfrac{E}{\tau_0}\left(\dfrac{f_t-\sigma_y}{E}\right)^2 & \text{for } \xi = 0 \end{cases} \tag{74}$$

When using Equation (74) it should be verified that the predicted crack opening w is less than w_{max} defined in the drop-constant stress-crack opening relationship applied (Equation (8)).

Once the crack opening has been determined the corresponding crack spacing may be found via Equation (71). The crack spacing will be in the interval $[l;2l]$. Note that the crack spacing increases with increasing w, thus, if we have large cracks they will be far apart, on the other hand, if we have narrow cracks they will be close together.

In Fig. 19 the normalized crack opening w/h is shown as a function of the residual strength σ_y. Two different slab materials are compared: one with a tensile strength of 3 MPa, the other with a 50% higher strength. The strength to stiffness ratio is assumed to be constant. It is observed that if the residual stress σ_y is the same in the two cases then the crack opening is larger when the tensile strength is higher. Note also that even for the same residual strength to tensile strength ratio, larger values of the crack opening are encountered when the tensile strength is increased.

A full scale test verifying the approach presented is described in [27] and experimental determination of the slab-sub base interface parameters τ_0 and ξ can be found in [24].

8. CONCLUSIONS AND DIRECTIONS FOR FUTURE WORK

In the present document the stress-crack opening relationship, $\sigma_w(w)$, is applied for designing steel fibre reinforced concrete structural elements involving cross-sections subject to combination of axial force, bending moment and shear force with or without conventional reinforcing bars. Furthermore shrinkage of slabs on grade is treated. The cross-sectional analysis with combined moment and axial force involves two main assumptions regarding:

1. The kinematic behaviour of the cracked cross-section.
2. Representation of the stress-crack opening relationship.

With respect to the first assumption, numerical calculations reveal that the overall structural response is insensitive to the kinematic assumptions.

With respect to the second assumption, the results of the uniaxial tensile test should guide the choice of the representation of the stress-crack opening relationship.

Since fibre orientation can change from one structural application to another, care must be taken to ensure that the chosen relationship is representative of the material in the structural application under consideration. In general, the more representative the stress-crack opening relationship is, the more comprehensive the prediction of the structural behaviour will be.

The design principles set forth in this document have been applied and verified in a number of studies, both experimental and numerical. Elements of experimental verification can be found in [6, 7, 20-22, 28].

Further work is needed in the following areas:

1. Further analyze situations involving mixed mode

crack propagation and opening (shear, torsion etc.).
2. Assess the sensitivity of the choice of analytical representation of stress-crack opening relationships.
3. Analyze the possibility of using the bending test as quality control in connection with the $\sigma_w(w)$ design method.
4. Assess time dependent effects such as fatigue, creep and durability.

BIBLIOGRAPHY

[1] RILEM Technical Committee TDF-162 'Test and design methods for steel fiber reinforced concrete. Recommendations for bending test' (Chairlady L. Vandewalle), *Mater. Struct.* **33** (225, January-February 2000) 3-5.

[2] RILEM Technical Committee TDF-162 'Test and design methods for steel fiber reinforced concrete. Recommendations for σ–ε design method' (Chairlady L. Vandewalle), *Mater. Struct.* **33** (226, March 2000) 75-81.

[3] RILEM Technical Committee TDF-162 'Test and design methods for steel fiber reinforced concrete. Recommendations for uni-axial tension test' (Chairlady L. Vandewalle), *Mater. Struct.* **34** (235, January-February 2001) 3-6.

[4] Bartos, P. J. M. and Duris, M., 'Inclined tensile strength of steel fibres in a cement-based composite', *Composites* **25** (November 1994) 945-951.

[5] Bélanger, A., 'Conception de dalles de ponts avec armature réduite et béton de fibres d'acier', Master's thesis, École Polytechnique de Montréal, 2000.

[6] Casanova, P. and Rossi, P., 'Analysis of metallic fibre-reinforced concrete beams submitted to bending', *Mater. Struct.* **29** (1996) 354–361.

[7] Casanova, P. and Rossi, P., 'Analysis and design of steel fiber reinforced concrete beams', *ACI Structural J.* **94** (5) (1997) 595-602.

[8] Cotterell, B. and Mai, Y. W., 'Fracture Mechanics of Cementitious Materials', Blackie Academic & Professional, Wester Cleddens Road, Bishopbriggs, Glasgow G64 2NZ, 1996.

[9] Dzeletovic, N., 'Propriétés des dalles de ponts avec béton de fibres', Master's thesis, École Polytechnique de Montréal, 1998.

[10] ENV-1992-1-1. Eurocode 2: Design of concrete structures - Part 1: General rules and rules for buildings. Technical report, 1992. European pre-standard.

[11] Hillerborg, A., 'Analysis of fracture by means of the fictitious crack model, particularly for fibre reinforced concrete', *The Int. J. Cem. Comp.* **2** (4) (1980) 177-184.

[12] Hillerborg, A., Modéer, M. and Petersson, P. E., 'Analysis of crack formation and crack growth in concrete by means of fracture mechanics and finite elements', *Cem. Concr. Res.* **6** (6) (1976) 773-782.

[13] Karihaloo, B. L., 'Fracture Mechanics and Structural Concrete', Concrete Design and Construction Series, Longman Scientific & Technical, Harlow, Essex, England, 1995.

[14] Kitsutaka, Y., 'Fracture parameters by polylinear tension-softening analysis', *J. Eng. Mechanics* **123** (5) (1997) 444-450.

[15] Kullaa, J., 'Fibre-reinforced concrete under uniaxial tension', *Nordic Concrete Research* **1/1994**(14) (1994) 77-90.

[16] Lange-Kornbak, D. and Karihaloo, B. L., 'Design of fiber-reinforced DSP mixes for minimum brittleness', *Advn. Cem. Bas. Mat.* **7** (1998) 89-101.

[17] Li, V. C., 'Post-crack scaling relations for fiber reinforced cementitious composites', *ASCE J. Mat. Civil Engng.* **4** (1) (1992) 41-57.

[18] Li, V. C., Stang, H. and Krenchel, H., 'Micromechanics of crack bridging in fiber reinforced concrete', *Mater. Struct.* **26** (162) (1993) 486-494.

[19] Maalej, M. and Li, V. C., 'Flexural strength of fiber cementitious composites', *ASCE J. of Mat. in Civil Eng.* **6** (1994) 390-406.

[20] Massicotte, B., Moffatt, K. and Bastien, D., 'Behaviour, analysis and design of fibre reinforced concrete structural members containing or not conventional reinforcement', Technical Report Report EPM/GCS-2001-10, Department of Civil, Geological and Mining Engineering, École Polytechnique de Montréal, 2001. In press.

[21] Massicotte, B. Bélanger, A. and Moffatt, K., 'Analysis and design of SFRC bridge decks' in Proceedings of the Fifth International RILEM Symposium Fibre-Reinforced Concretes (FRC), BEFIB' 2000 (P. Rossi and G. Chanvillard, Editors), RILEM Publications S.A.R.L. (Cachan, France) (2000) 263–272.

[22] Moffatt, K., 'Calcul des dalles de pont avec béton de fibres d'acier', Master's thesis, École Polytechnique de Montréal, 2001.

[23] Nanakorn, P., Horii, H. and Matsuoka, S., 'A fracture mechanics-based design method for SFRC tunnel linings', *J. Materials, Conc. Struct., Pavements* **30** (532) (1996) 221-233.

[24] Olesen, J. F., 'FRC slabs on grade, full-scale tests', 1999. Department of Structural Engineering and Materials, Technical University of Denmark, MUP2.

[25] Olesen, J. F., 'Cracks in reinforced FRC beams subject to bending and axial load', in 'Fracture Mechanics of Concrete Structures' (R. de Borst, J. Mazars, G. Pijaudier-Cabot and J. G. M. van Mier, Editors), A. A. Balkema Publishers (2001) 1027-1033.

[26] Olesen, J. F., 'Fictitious crack propagation in fiber-reinforced concrete beams', *Journal of Engineering Mechanics* **127** (3) (March 2001) 272-280.

[27] Olesen, J. F. and Stang, H., 'Designing FRC slabs on grade for temperature and shrinkage induced cracks', in Proceedings of the Fifth International RILEM Symposium Fibre-Reinforced Concretes (FRC), BEFIB' 2000 (P. Rossi and G. Chanvillard, Editors), RILEM Publications S.A.R.L. (Cachan, France) (2000) 337-346.

[28] Pedersen, C., 'New production processes, materials and calculation techniques for fiber reinforced concrete pipes', PhD thesis, Department of Structural Engineering and Materials, Technical University of Denmark, Series R, no. 14, 1996.

[29] Rossi, P., 'Steel fiber reinforced concrete (SFRC): An example of French research', *ACI Mat. J.* **91** (3) (May-June 1994) 273-279.

[30] Rossi, P. and Harrouche, H., 'Mix design and mechanical behaviour of some steel-fiber reinforced concretes used in reinforced concrete structures, *Mater. Struct.* **23** (1990) 256-266.

[31] Shah, S. P., Swartz, S. E. and Ouyang, C., 'Fracture Mechanics of Concrete', John Wiley & Sons Inc., New York, 1995.

[32] Stang, H. and Aarre, T., 'Evaluation of crack width in FRC with conventional reinforcement', *Cement & Concrete Comp.* **14** (2) (1992) 143-154.

[33] Stang, H. and Olesen, J. F., 'On the interpretation of bending tests on FRC-materials' in Proceedings FRAMCOS-3, volume 1, Fracture Mechanics of Concrete Structures, (H. Mihashi and K. Rokugo, Editors) Aedificatio Publishers (D-79104 Freiburg, Germany) (1998) 511-520.

[34] Stang, H. and Olesen, J. F., 'A fracture mechanics based design approach to FRC' in Proceedings of the Fifth International RILEM Symposium Fibre-Reinforced Concretes (FRC), BEFIB' 2000 (P. Rossi and G. Chanvillard, Editors), RILEM Publications S.A.R.L. (Cachan, France) (2000) 315-324.

[35] Ulfkjær, J. P., Krenk, S. and Brincker, R., 'Analytical model for fictitious crack propagation in concrete beams', *ASCE, J. Eng. Mech.* **121** (1) (1995) 7-15.

[36] Vandewalle, L., 'Cracking behaviour of concrete beams reinforced with a combination of ordinary reinforcement and steel fibers', *Mater. Struct.* **33** (April 2000) 164-170.

Appendix

Numerical comparison of methods for beam analysis

As an example, the beam analysis described in section 5 has been carried out with the simplified non-linear hinge analysis of [28] and the explicit non-linear hinge analysis of [26]. In both models $s = h/2$ is used. Furthermore, the models of [7], which assume a parabolic curvature variation and a non-linear hinge with varying length (see Equation (23)), and [20] using a model adopting a constant hinge length and a constant curvature over the non-linear hinge, were adopted. The deflection of the beam was obtained through the numerical integration of the moment curvature response in the models of [7]and [20], while the approach outlined in section 5 was adopted in the calculations based on the models of [28] and [26].

Also a non-linear fracture mechanics analysis has been carried out using the finite element program DIANA with discrete interface elements. The finite element program is able to handle a bi-linear stress-crack opening curve.

The analysis has been carried out on a beam with cross sectional dimensions h = 150 mm and b = 150 mm. Two different spans were considered: L = 500 mm and L = 1000 mm. In all types of analysis the same bi-linear stress-crack opening relation (7) with the parameters given in Table 1 was used. Young's modulus E was assumed to be 35 GPa.

Table 1 – The material parameters describing the bi-linear stress-crack opening relationship used in the present comparison between different types of analysis

f_t (MPa)	α_1 (MPa/mm)	σ_2 (MPa)	α_2 (MPa/mm)
3	30	1.5	0.15

The results of the calculations are given in Figs. 20 and 21, where both the $P(u)$ and the $w_{cmod}(u)$ are shown for both beams. Overall the agreement between the different methods is good. As shown it is practically impossible to distinguish between the three non-linear hinge approaches of [20, 26 and 28]. The FEM analysis shows good agreement with the non-linear hinge approach.

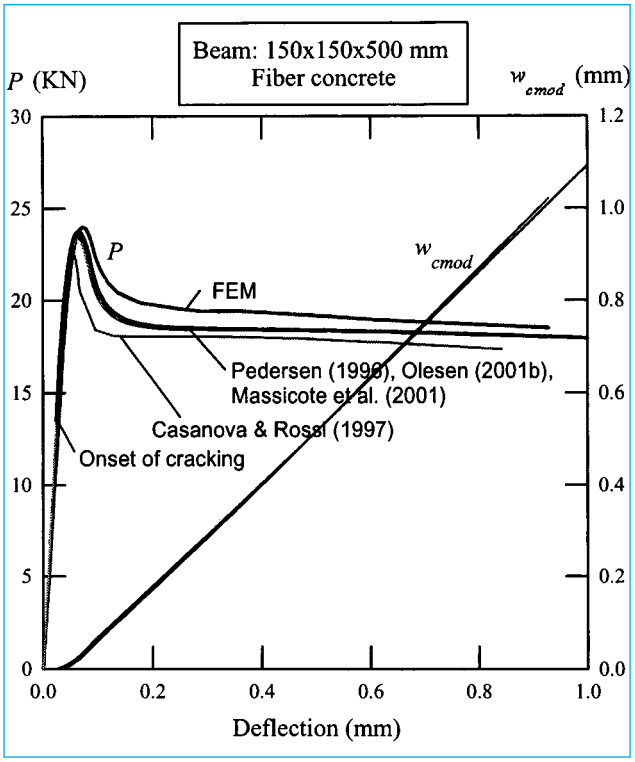

Fig. 20 - The results of the calculations of the load-deflection and w_{cmod}-deflection diagrams for the short beam. The analytical results for the load-deflection diagram are shown using the models of [7, 20, 26, 28]. Shown is also a FEM analysis using the discrete crack approach with the program DIANA. In general the analytical results fall slightly below the results of the FEM analysis. The results using the models of [20, 26, 28] are so close that the curves cannot be distinguished. The w_{cmod}-deflection diagram is shown only for the FEM analysis and the model of [28]. In this case the FEM analysis and the analytical model give very similar results.

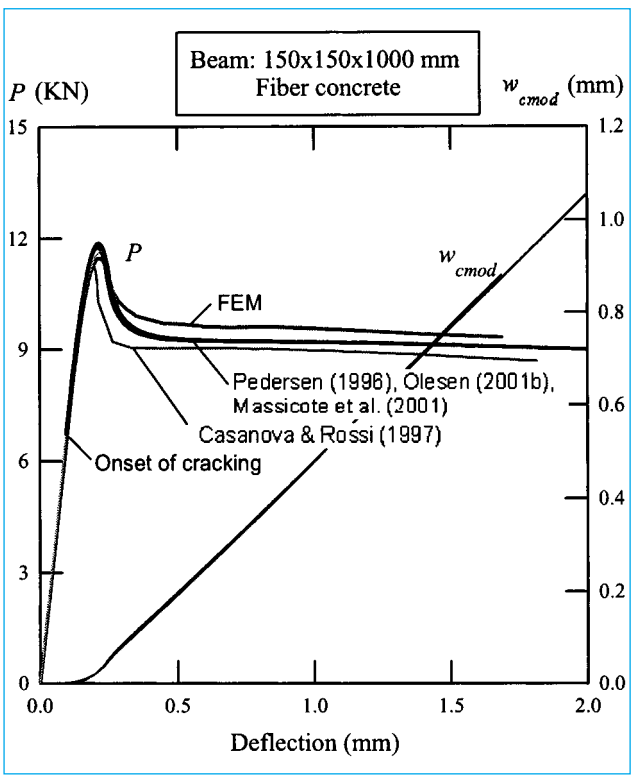

Fig. 21 – The results of the calculations of the load-deflection and w_{cmod}-deflection diagrams for the long beam. A comparison between the different approaches leads to conclusions similar to the conclusions in the case of the short beam.